Limits of the quasiharmonic approximation in MgO: Volume dependence of optical modes investigated by infrared reflectivity and ab initio calculations

Eugenio Calandrini, Lorenzo Paulatto, Daniele Antonangeli, Fei He, Ricardo Lobo, Francesco Capitani, Jean-Blaise Brubach, Pascale Roy, Laetitia Vincent, Paola Giura

Limits of quasiharmonic approximation in MgO: volume dependence of optical modes investigated by infrared reflectivity and *ab initio* calculations

Eugenio Calandrini[1], Lorenzo Paulatto[1], Daniele Antonangeli[1], Fei He[1], Ricardo P. S. M. Lobo[2,3], Francesco Capitani[4], Jean-Blaise Brubach[4], Pascale Roy[4], Laetitia Vincent[5], and Paola Giura[1*].

[1] *Sorbonne Université, Museum National d'Histoire Naturelle, UMR CNRS 7590, Institut de minéralogie, de physique des matériaux et de cosmochimie (IMPMC), 4 place Jussieu, F-75005 Paris, France*

[2] *LPEM, ESPCI Paris, PSL Univeristy, CNRS, F-75005 Paris, France*

[3] *Sorbonne Université, CNRS, LPEM, F-75005 Paris, France*

[4] *Synchrotron Soleil, L'Orme des Merisiers Saint Aubin, BP 48 91192, Gif-sur-Yvette , France*

[5] *Université Paris-Saclay, CNRS, Centre de Nanosciences et Nanotechnologie, C2N, Palaiseau 91120, France*

ABSTRACT

Experimental and numerical investigation of phonon optical modes of MgO as a function of temperature (from 300 to 1400 K) and pressure (from 0 to 21 GPa) are here presented. Infrared reflectivity measurements were performed to probe energies and widths of the optical phonons, as well as of the multiphonon processes affecting the spectral shape, over a variation of the unit cell volume exceeding 20%. Calculations within quasi harmonic approximation (QHA) account well for the volume dependence of the optical phonon energies observed in high-pressure experiments, while they fail at larger volumes, corresponding to the highest investigated temperatures. Moreover, QHA calculations more closely predict energies of transverse optical (TO) modes than those of longitudinal optical (LO) ones. This can be ascribed to known limitations in the modeling of the effective charges (Z^*) and dielectric constant (ε_∞) that lead to an underestimation of the LO-TO splitting. Based on the comparison of our experimental and theoretical results, we propose an empirical analytical expression for $Z^{*2}/\varepsilon_\infty$ as a function of the atomic cell volume. Density-functional perturbation theory including phonon-phonon scattering up to the third order of the lattice potential expansion is used to calculate phonon widths. These calculations reproduce and explain remarkably well the non-trivial volume dependence of both TO and LO phonons linewidths determined by the experiments.

Introduction

Lattice dynamics controls many of the physical quantities responsible for the thermodynamic properties of condensed matter. Among them, we found entropy, thermal capacity, specific heat, thermal expansion, and thermal conductivity [1]. To be able to interpret, predict, and eventually modify these physical quantities in actual materials, is essential to establish an accurate enough model of the force fields, velocities, and scattering rates responsible for atomic movement [2]. This has motivated an advanced treatment of the interatomic potential in which the anharmonic terms are explicitly considered.

Anharmonicity of the interatomic potential leads the interactions between phonons and is therefore responsible for their mutual scattering. Several microscopic descriptions have been developed to explain anharmonic forces and their contribution to intrinsic phonon-phonon scattering processes, either based on experimental data [3], or first principles approaches [4–10]. However, further refined experiments and advanced calculations are needed to adequately understand multiphonon scattering and its impact on the physical properties of solids [11–16].

To this end, infrared spectroscopy is a first-choice technique to directly address anharmonicity by probing the energy and the lifetime of the infrared active lattice modes. In a purely harmonic picture for diatomic cubic crystals, the infrared absorption spectra should consist of one narrow line. In reality, the measured infrared spectra of cubic crystals show a broad band and at least a secondary band [17]. This discrepancy is qualitatively attributed to anharmonic terms in the potential energy. Thanks to them, the interaction between lattice modes becomes possible, so that a combination of two or more lattice waves can absorb in the infrared region even when the individual waves cannot. Within this context, simple materials, such as the insulating, rock salt structured

*corresponding author: paola.giura@sorbonne-universite.fr

Magnesium Oxide (MgO) provide an ideal playground, both for experiments (high-quality samples are commercially available) and calculations (with its 2 atoms per unit cell and 6 phonon branches it is not computationally demanding, allowing more complex, detailed, and realistic calculations). Furthermore, the stability of MgO, which retains the NaCl (B1) structure over several megabars and thousands of degrees ([18] and references therein), can be exploited to vary interatomic distances by either pressure or temperature, independently tailoring the phonon-phonon coupling as it will be seen in the following.

An improved understanding of the properties of MgO has also direct implications for Earth and planetary science, being MgO the compositional end-member of ferropericlase $(Mg_{1-x},Fe_x)O$, one of the most abundant constituents of the Earth's lower mantle [19–21] and planetary mantles at megabar pressures [22]. In particular, vibrational properties of MgO and $(Mg_{1-x},Fe_x)O$ are directly relevant for the interpretation of lower mantle seismological observations [23–25] and to model the heat transfer across the planet [4,5,26–28]. In addition, MgO has a technical relevance since it is widely employed as a substrate in chips for THz devices [29].

Despite such a great and diversified interest, MgO vibrational properties as a function of temperature and pressure are relatively poorly known. This paper focuses on the study of the intrinsic phonon-phonon scattering (phonon anharmonicity) and its impact on the normal optical modes in terms of their energies and widths. The evolution with pressure and temperature of these dynamical parameters is here monitored over variations in the unit cell volume of 20% by a combined experimental and theoretical approach. Interestingly, the rearrangement of the phonon density of states at high pressure triggers multiphonon processes that increase the linewidth of the longitudinal modes. Finally, the here-presented methodological approach can be extended to the study of the thermoelastic properties and of the lattice thermal conduction of other insulating crystals of geophysical or technological interest.

Methods

Infrared reflectivity measurements have been performed on MgO single crystals as a function of temperature and pressures in multiple runs, exploiting different instruments and experimental configurations [See Supplemental Material]. High-quality data have been collected between 300 and 1400 K at ambient pressure, and between 0 and 21 GPa at ambient temperature. While measurements covered a larger spectral range, features of current interest locate in the 200 to 1000 cm^{-1} range.

Experiments have been complemented by lattice dynamics calculations implemented in the QUANTUM ESPRESSO suite [see supplemental Material].

Experimental and Computational Results

The reflectance spectra of MgO measured as a function of temperature and pressure are shown in Figures 1a and b, respectively. All spectra are characterized by a frequency band of high reflectivity, the so-called reststrahlen band. The transversal and longitudinal optical phonon frequencies at almost zero wave vector, ω_{TO} and ω_{LO}, limit this band. These frequencies relate to the normal modes of lattice vibrations. Outside this spectral region, the reflectivity is constant. The fringes in the high-pressure measurements are due to the multiple internal reflections inside the pressure chamber. The reststrahlen band is perturbed by a shoulder at a frequency slightly lower than ω_{LO}, whose nature goes beyond the quasi-harmonic approximation of lattice dynamics, and can be ascribed to anharmonic phonon-phonon interactions as discussed in detail in a recent work [31]. Briefly, this shoulder is the signature of an Excess of Spectral Weight (ESW) due to the decay of a photon with energy $\hbar\omega_{ESW}$ and vanishing wavevector ($q_{in}\sim 0$) in two phonons with opposite wavevector (q_{out}, $-q_{out}$), whose energies sum up to $\hbar\omega_{ESW}$. These multiphonon processes are particularly pronounced in ionic compounds, such as MgO, for which the peculiarities of the phononic band structure allow a discretization of the density of state and the onset of pockets, favorable to the phonon-phonon interaction [31].

Overall, spectra undergo a continuous redshift upon increasing temperature and blueshift with increasing pressure. To better highlight this behavior, ω_{TO}, $\omega_{LO,}$ and ω_{ESW} frequencies are marked by colored points in the spectra shown in Figure 1. A useful way to look at this is by considering, rather than temperature and pressure, the lattice volume, which systematically increases by moving from the bottom to the top of Figure 1. Qualitatively, phonon softening is commonly expected with increasing interatomic distances. The softening of the ESW energy is a consequence of the general phonon energies shift over the entire reciprocal space, which effectively moves toward lower energies the high phonon density of state pockets responsible for the ESW.

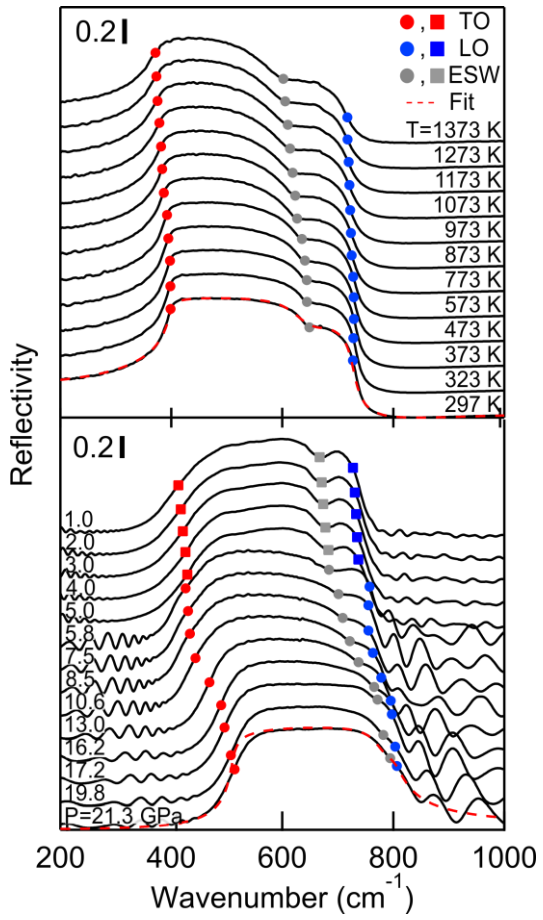

Figure 1 Reflectivity spectra of MgO single crystal as a function of temperature (top) and pressure (bottom). The curves are all rigidly vertically shifted by the same amount (0.2) for better visibility. The red dashed curves are representative fit results. Red, blue, and gray symbols highlight the position of TO and LO phonons and the ESW feature, respectively. Circles and squares are for different experimental runs.

The thermodynamic behavior of the aforementioned lattice excitations and their lifetimes can be quantitatively described by retrieving the dielectric function of MgO, which directly relates to the refractive index. Results have been analyzed both according to a Lorentz model, and when possible, based on the Kramers-Kronig relation [Supplemental Material] [32,33]. As illustrated for the high-temperature measurements (Figure 2a-e), both the Lorentz model (in black) and the Kramers-Kronig relations (in red) capture the relevant features of the dielectric function of the system, and only differ at the edge of the investigated ranges. Concerning the high-pressure measurements, the unavoidable fringes hamper the Kramers-Kronig analysis. As such, in the following, the analysis will be based on the Lorentz model. Representative curves of this fitting procedure are superimposed to the corresponding measured spectra as red dashed lines in Figure 1.

Knowing the dielectric constant, the imaginary part of the energy loss function $\varepsilon_2/(\varepsilon_1^2 + \varepsilon_2^2)$ provides the frequency and linewidth of LO phonons. The results of this approach are presented in Figure 2, where ε_2 is shown in panels (a) and (c) and the imaginary part of the energy loss function in panels (e) and (g) for high temperature and high pressure, respectively.

As already mentioned, the peaks' blue shift with decreasing volume (going from top to bottom) is clearly visible. In particular, the ESW peak exhibits a larger shift than the phonons peaks, so that at high pressure it crosses the LO (panel (g)). The evolution of peak linewidths can also be directly inferred. As expected, a general broadening is observed at high temperature for all the considered excitations. Conversely, TO and ESW linewidths remain constant at high pressure, while the LO linewidths unexpectedly increase.

These experimental results can be directly compared with the density functional perturbation theory (DFPT) calculations. The resolution of the exact ionic Hamiltonian, using harmonic phonons as the basis, and perturbatively threatening the third order of the total energy approximation, provides corrections to the phonon self-energy, which acquires an imaginary part and confers to the phonons a finite lifetime, i.e., an intrinsic linewidth. The calculated spectral functions of TO and LO phonons take into account these corrections and are displayed in Figure 2b-2f and Figure 2d-2h for temperatures and pressures between 300 and 1473 K and 0 and 40 GPa, respectively. The agreement with the experiments [in panels (a),(c),(e) and (g) of Figure 2] is remarkable.

Calculations directly provide the energies and linewidths of normal modes. More interestingly, the analysis of the spectral functions of panels (b),(d), (f) and (h) of Figure 2 also allows addressing multiphonon processes. Two extra bands, on top of that corresponding to normal models, are well visible. The first (indicated with a star symbol) is the ESW, several orders of magnitude weaker than the normal modes. The second one, further out, is even weaker and highly structured. As the latter lies outside the reststrahlen band, reflectivity measurements are of little use for its investigation, all the more in the case of high-pressure measurements, as the fringes complicate the data interpretation. Thus, while we will discuss here ESW related features, we defer the analysis of this second extra band to further dedicated studies. However, it is worth noticing that DFPT calculations can reveal these multiphonon processes, and the discrepancies between the Lorentz model and the Kramers-Kronig analysis at high wavenumbers (Figure 2(a)-2(e) can be related to the omissions of such

processes. The ω_{ESW} frequency is assigned evaluating the local maximum of σ_{TO} and rapidly crosses the ω_{LO} frequency, as can be seen in panels (f) and (h) of Figure 2. This complicates the analysis of the imaginary part of the energy loss function because for certain thermodynamic conditions the ω_{LO} and ω_{ESW} modes are closer than the respective linewidths.

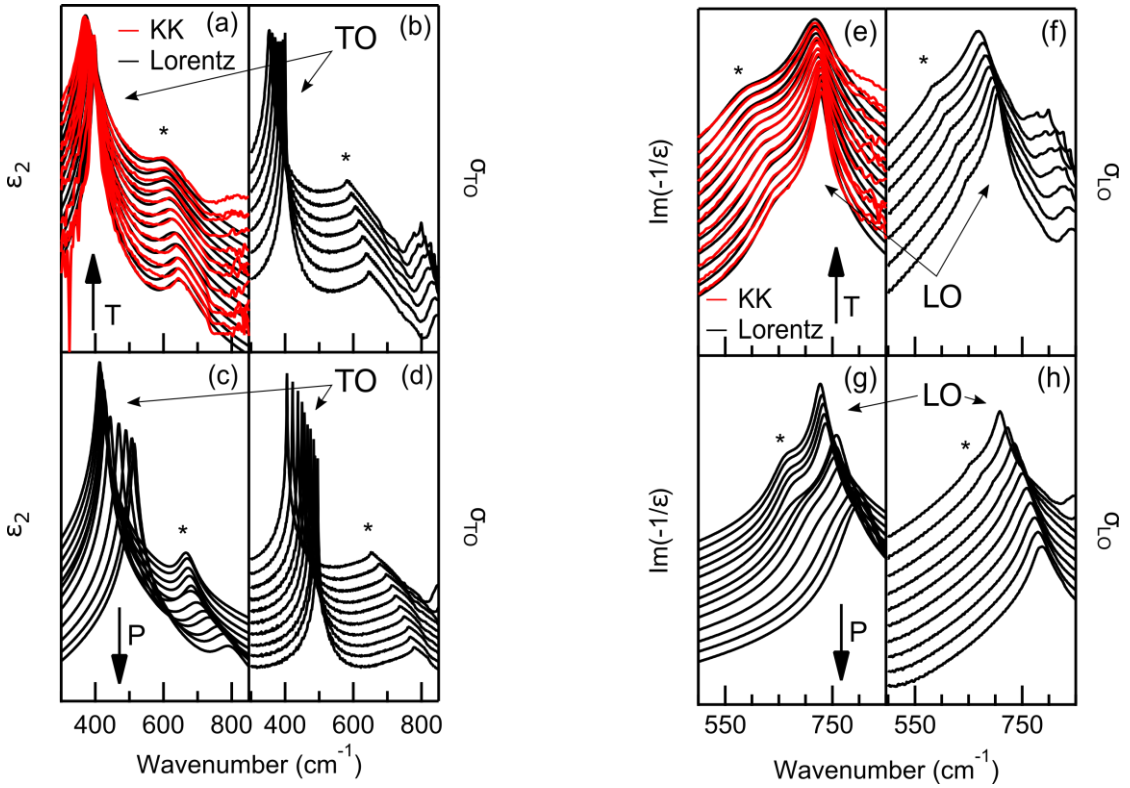

Figure 2: Experimental and computed optical function of MgO. Panel (a), (c), (e) and (g) show the experimental data analysis results: Lorentz fit (black curves) and Kramers Kronig analysis (red curves). Panel (a) and panel (c) show the imaginary part of the dielectric function ε_2 at high temperature (a) and high pressure (c). Panel (e) and panel (g) shows the energy loss function at high temperature (e) and high pressure (g). Panel (b), (d), (f) and (h) show the calculated spectral function of TO and LO at high temperature (b, f) and high pressure (d, h). N.B. The ordinate axes are in logarithmic scale. Stars (*) indicate the ESW structure. The main features due to the transverse and to the longitudinal optical phonon are indicated by arrows. Temperature (top panels) increases from the bottom to the top. Pressure (bottom panels) increases from the top to the bottom. Curves are staggered for better visibility.

Both experimental and numerical results on TO, LO, and ESW are summarized in Figure 3, where the frequencies and linewidths are displayed as a function of lattice volume (bottom axis) and as a function of temperature and pressure (top axis). The agreement on phonon energies between experiments and calculations, and their smooth, almost-linear dependence on lattice volume, indicate that the quasi-harmonic approximation is suitable to describe the lattice dynamics of the system over an extended volume range. Some discrepancies exist concerning LO phonon energy, which results in an underestimation of the theoretically computed LO-TO splitting. This is a known limitation, deriving from the energy functional approximation used to calculate the electronic ground state of the system. However, this problem can be overcome, as discussed later on.

Very differently, the TO and LO phonons linewidths show a non-trivial dependence on the lattice volume [Figure 3(b)]. Here the anharmonic treatment of the problem is needed to recover the overall behavior of linewidths and its non-monotonic dependence on lattice volume. Even if the absolute values do not closely match, the increases in the TO and LO phonon linewidths by almost a factor of 3 at large volumes are well reproduced. Noteworthy, since the mismatch is uniform for both the modes, it is conceivable to ascribe this to extrinsic origins. Adding scattering due to isotopic disorder into our calculations does not significantly affect resulting linewidths. Experimentally observed broadening

could thus be due to point defects, or other scattering sources.

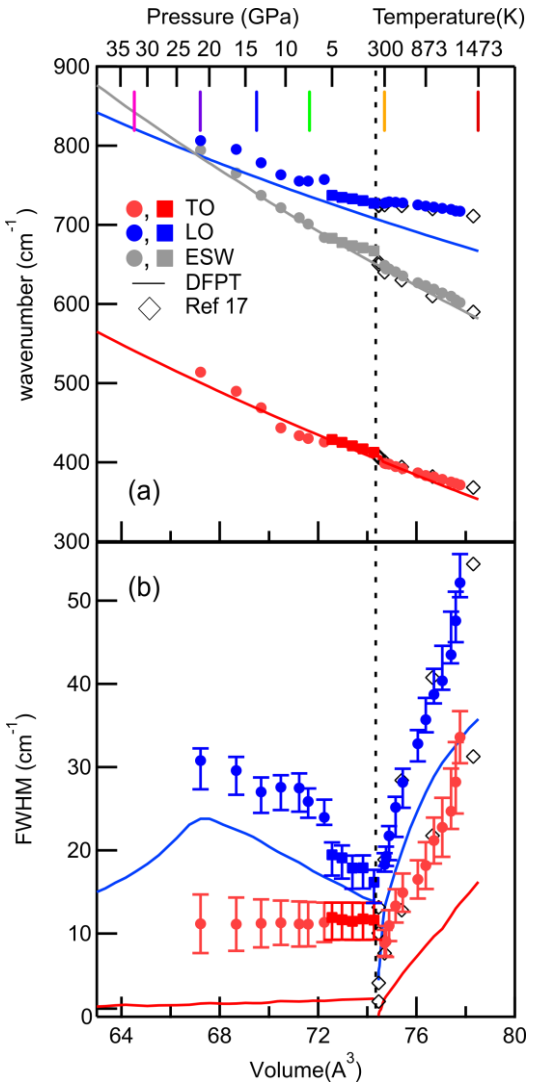

Figure 3. (a) Phonon energies calculated in the quasi-harmonic approximation (lines) and extracted from the Lorentz fit of recorded spectra (circles and squares). (b) Phonon widths calculated including the third order (lines) and extracted from the Lorentz fit of recorded spectra (circles and squares). Literature data from [17] are reported as open diamonds. Colored markers correspond to P-T conditions at which we performed phonon DoS and Final State calculations reported in Figure 7. To assign an experimental error, the Lorentz fits were repeated after a rescaling of the measured reflectivity of ± 1%. This procedure reduces any errors caused by the uncertainty on the absolute intensity of the single spectrum and minimizes the effects of misalignment intrinsic to the acquisition of the background. This approach produced the reported error bars for the phonon widths, while no significant effect was produced on the phonon energies.

Discussion

Modes energies

Figure 3 compares the volume dependence of ω_{TO} and ω_{LO} obtained by experiments and by *ab-initio* simulations. Despite the scatter in the experimental data, it is possible to appreciate the good agreement between experiments and QHA simulations up to a critical volume, above which calculations start to deviate from measurements (please refer to Supplemental Material Figure S1 for a closer comparison). For the longitudinal phonon, deviation starts at volumes corresponding to room pressure - room temperature measurements, while for the transverse phonon, deviation occurs at higher volumes, indicating a more harmonic behavior with respect to the longitudinal mode. Also, while calculations fit well the experimental transverse energies, longitudinal energies are systematically underestimated. As better addressed in the next section, this is a direct consequence of the difficulties in reproducing the effects of the mean local electric field associated with the long-wavelength limit longitudinal phonon.

A first interesting observation that can be made by considering the experimental results at around V=74.1 Å^3 (gray shaded area in Figure S1) is that the energy of the optical modes measured at moderate pressures (~ 1 GPa) and room temperature (full circles) is, within uncertainties, the same energy of the optical modes measured for the same volumes, but at ambient pressure and low temperature (< 300K) (open circles from ref. [33]). As expected within a quasi-harmonic approximation, volume seems to be the thermodynamic variable controlling the dynamics, irrespective of actual pressure and temperature conditions leading to this volume. It may therefore be instructive to see over which volume range such observation holds, or in other words, to find the limits above which the quasi-harmonic approximation cannot be satisfactorily used anymore.

QHA calculations reproduce well the overall energy-volume relations observed in the high-pressure experiments (but for a rescaling of the absolute values of LO), suggesting that a quasi-harmonic approximation holds at ambient temperature at least up to 22 GPa, corresponding to a volume of 67.22 Å^3. High volumes, obtained for ambient pressure and high temperatures, are more critical, and QHA calculations fail at reproducing the energy-volume relations established by our experiments and available literature data [17]. The difference between experiments and calculations is already sizable at 373 K (74.87 Å^3) for LO and becomes evident at 773 K

(76.05 Å ^{3}) for TO as well (Figure 3 and Figure S1 in Supplemental Material). Thus, the quasi-harmonic approximation does not provide an appropriate description of the system at ambient pressure and high temperature.

To further characterize the limits of validity of the quasi-harmonic approximation measurements obtained at constant volume for a different combination of pressure and temperature are necessary (e.g. [35]). To the same extent, it will be worth to perform perturbative calculations, in particular at high temperature, including both third and fourth orders in the development of the phonon self-energy, which antagonistically contribute to phonon energy determinations, and whose relative weights are expected to depend on actual thermodynamic conditions.

LO-TO splitting

While first principle calculations well predict the energy of the TO phonons, computed values of the LO energies are systematically below the measured ones (Figure 3). This problem can be partially solved by empirical corrections based on the analysis of LO-TO splitting.

The LO-TO splitting, *i.e.* the removal of degeneracy between the LO and TO phonons at the Brillouin zone center, arises from the breaking of the lattice symmetry by the long-range electric fields associated with long-wave longitudinal phonons. This effect can be accounted for in the dynamical matrix as $q \to 0$, introducing a non-analytic contribution given by:

$$\frac{4\pi}{\mathrm{V}} e^2 \frac{(q\cdot Z_i^*)_\alpha (q\cdot Z_j^*)_\beta}{q\cdot\varepsilon_\infty\cdot q}, \qquad (3)$$

where V is the volume of the primitive cell, $Z^*_{i(j)}$ is the Born effective charge tensor for the *i(j)-th* atom, ε_∞ is the high-frequency static dielectric tensor, and e is the electronic charge. Thus, the knowledge of the tensor Z^* of the Born effective charges and the tensor ε_∞ of the macroscopic high-frequency dielectric constant is needed to correctly describe the dynamical matrix at the Brillouin zone center. Actually, the ratio $Z^{*2}/\varepsilon_\infty$ controls the magnitude of the LO-TO through the relation:

$$\frac{Z^{*2}}{\varepsilon_\infty} = \frac{\mu \mathrm{V}}{4\pi e^2}(\omega_{LO}^2 - \omega_{TO}^2) \qquad (4)$$

where μ is the reduced atomic mass and V the volume of the unit cell. The values for Z^* and ε_∞ can be self-consistently calculated in the framework of DFPT, but also derived from the experiments. In the latter case, the high-frequency dielectric constant is a fit parameter, while the Born effective charges can be determined by the following relation:

$$Z^{*2} = \frac{\mu \,\mathrm{VS}\, \omega_{TO}^2}{4\pi e^2}, \qquad (5)$$

where μ is the reduced mass of MgO, V is the volume of the unit cell, S and ω_{TO}^2 are respectively the oscillator strength and frequency of the transverse phonon, and e is the electronic charge.

Figure 4 compares the measured and calculated values for Z^*, the tensor ε_∞ and the ratio $Z^{*2}/\varepsilon_\infty$. In particular, the $Z^{*2}/\varepsilon_\infty$ experimental values shown in Figure 4 are obtained by the Lorentz model analysis used to estimate:

i) the mean value of the high-frequency dielectric constant, ε_∞ (Figure 4, inset (a)) from the high-energy trend of the mean reflectivity curve obtained by averaging the experimental data at the different volumes.

ii) the effective charge number Z* (Figure 4, inset (b)) from the transverse optic phonon oscillator strength.

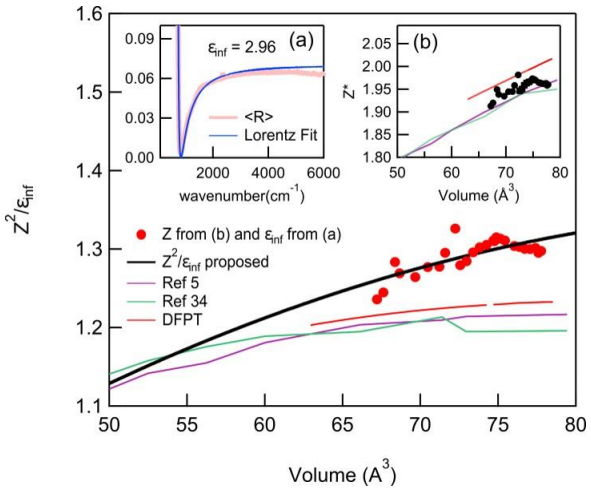

Figure 4. Ratio $Z^{*2}/\varepsilon_\infty$ as a function of volume. The estimation from experimental results (dots) is compared to estimations from the *ab-initio* simulations (thin lines) performed in this study (DFPT) and available in the literature [5,34]. Inset (a): Lorentzian fit (blue line) of the high-energy trend of the mean reflectivity curve <R> (red line). Inset (b): effective charge number Z*.

In spite the present *ab-initio* calculations plot closer to the experimental determination than previous work [5,34], computed $Z^{*2}/\varepsilon_\infty$ are systematically below the experimental values. This

discrepancy mostly comes from the overestimation of the high frequency dielectric constant and not from the Born effective charge (Inset (b) of Figure 4), as also evidenced by the systematic underestimation of the longitudinal optical mode energy shown in Figure 3. In particular, all theoretical models underestimate the increasing LO-TO splitting with increasing volume.

To improve the accuracy of the theoretical modeling and to minimize the difference with respect to measurements, a $Z^{*2}/\varepsilon_\infty$ ratio scaled on the experimental data can be treated as an external input parameter for the calculations. Starting from a polynomial fit to the experimental values (bold thick black line in Figure 4), we can define an empirical analytical expression for $\left(Z^{*2}/\varepsilon_\infty\right)_{Exp}$ as a function of the atomic unit cell volume V:

$$\left(Z^{*2}/\varepsilon_\infty\right)_{Exp}(V) = 0.4(2) + 1.9(1)\cdot 10^{-2}\,V - 9.7(4)\cdot 10^{-5}\,V^2 \quad (6)$$

Such empirical scaling is neither meant to replace more advanced treatments of the dynamical matrix in the limit of $q \to 0$, nor of the Born effective charge tensor over an extended pressure or temperature range. Here we simply aim at providing an analytical correction to be applied to estimation of the LO-TO splitting by quasi-harmonic calculations over the here-considered volume range, and within the limit of a quasi-harmonic approach.

Grüneisen parameters

A classic, but still largely used way to describe and to quantify anharmonicity is through the Grüneisen parameter (γ) [36]. In this microscopic picture of the lattice dynamics, atomic oscillations are controlled by a pair potential energy containing an attractive and a repulsive term, which depend on the relative mean distance between the atoms. At finite, but relatively low temperature, the atomic displacement is sufficiently small with respect to the interparticle distances, so that the potential energy around the equilibrium position could be satisfactorily approximated by a parabola giving rise to an elastic recovering force (pure harmonic model). In the Grüneisen description, the equilibrium position is a function of temperature and pressure to account for the volume variation caused by thermal expansion or by compression (*quasi*-harmonic approximation). Noteworthy, in this model the only influence of pressure and temperature on the vibrational frequency comes from the effect that these have on the interatomic equilibrium position, or in other terms, on the volume *V*. These arguments and approximations lead to the classically used equations:

$$\frac{1}{\upsilon}\frac{\partial \upsilon}{\partial T} = -\gamma\frac{1}{V}\frac{\partial V}{\partial T} \quad (7)$$

$$\frac{1}{\upsilon}\frac{\partial \upsilon}{\partial P} = -\gamma\frac{1}{V}\frac{\partial V}{\partial P} \quad (8)$$

$$-\frac{\partial \ln(\upsilon)}{\partial \ln(V)} = \gamma \quad (9)$$

where γ is the Grüneisen parameter that can be written for every phonon mode as follows:

$$\gamma_i = -\frac{\partial \ln(\upsilon_i)}{\partial \ln(V)}, \quad (10)$$

where υ_i refers to the frequency of the *i-th* phonon mode.

From a macroscopic standpoint, the Grüneisen parameter is defined as [37]:

$$\gamma = \frac{\alpha K_T V}{C_V} = \frac{\alpha K_S V}{C_p} \quad , \quad (11)$$

where K_T (K_S) is the isothermal (adiabatic) bulk modulus, α is the thermal expansion coefficient and C_V (C_p) is the specific heat at constant volume (pressure). From equation 11, one can see that the Gruneisen parameter sets a link between the thermal and the elastic properties of a solid.

Figure 5 shows the natural logarithm of the phonon energy of the optical modes probed in this study, ln(ω_{LO}) (red) and (ω_{TO}) (blue), as a function of ln(V) for both high-pressure and high-temperature ranges. To facilitate comparison, quantities are rescaled to their respective values at ambient conditions, *i. e.* T=300 K and P= 1 atm (V= 74.704 Å^3, ω_{LO}=727 cm^{-1} and ω_{TO}=400 cm^{-1}). At high pressures (low volumes) QHA calculations well account for the observations, within the scatter of the data. Conversely, a departure from the quasi-harmonic model can be noticed at high temperature, with increasing volumes, at first for LO, then for TO. Over this volume range, both LO and TO data can be well described by a linear fit (dashed lines in Figure 5), whose slope is less steep than what is expected according to QHA calculations.

It can also be readily observed that the energy of the transverse mode has a more pronounced dependence on the volume than the energy of the longitudinal one. This can be rationalized by considering the effect of atomic distances on the Coulomb force associated with the long-range electric fields at the origin of the LO-TO splitting: with increasing/decreasing interatomic distances

(increasing/decreasing volume) the Coulomb force decreases/increases.

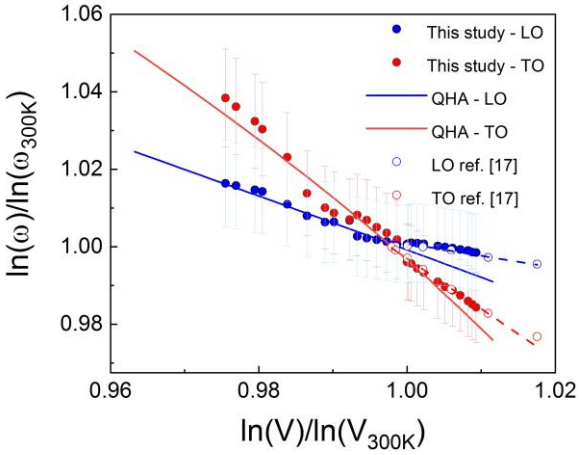

Figure 5. Natural logarithm of the phonon energy ω_{LO} (red) and ω_{TO} (blue) as a function of ln (V) for high-pressure and high-temperature measurements (dots) and QHA calculations (solid lines). Linear fits for the high-volume (HV) experimental data, there where the QHA calculations do not account for the experimental observations anymore, are displayed as dashed lines with consistent color-coding.

The greater hardening of the TO mode with decreasing volume is also clearly described by the Grüneisen parameter, calculated according to equation (10), and whose trend with volume is reported in Figure 6. In the volume range where QHA calculations well describe the measurements, $\gamma(V)_{QHA}$ follows a quadratic law much more pronounced for the transverse optical phonon than for the longitudinal one. At higher volumes, we estimated the mode Gruneisen parameters starting from the linear fit to the experimental data (dashed lines in Figure 5). In this volume range, γ_{TO} is more than 3 times γ_{LO}.

By looking at Figure 6, it is possible to remark that, within the quasi-harmonic approach, Grüneisen parameters decrease with reducing volume. Such behavior is consistent with high-pressure measurements, but it becomes soon inadequate for the high-temperature measurements. At the high volumes, corresponding to the highest temperature conditions, $\gamma(V)$ strongly decreases for both modes while the relative ratio between $\gamma(V)_{TO}/\gamma(V)_{LO}$ increases (see inset in Figure 6).

Quantitatively, although with a discontinuity likely less sharp than what schematically illustrated in Figure 6, the Gruneisen parameter for the longitudinal phonon goes from ~ 1 to ~ 0.3, a value three times smaller, while that of the transverse phonon changes by less than half passing from ~ 2.2 to ~ 1.3.

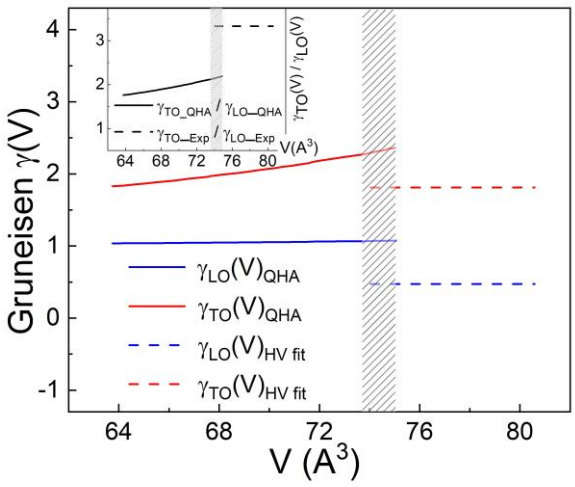

Figure 6. Gruneisen parameters for LO (blue) and TO (red) phonons as a function of volume. Continuous lines are QHA results, dashed lines are obtained by the derivative of the fits to the experimental data at the high volumes (dashed lines in Figure 5). The shaded region highlights the high volume (HV) range over which QHA calculations progressively deviate from experimental observations. Inset: TO/LO Grüneisen parameters ratio.

This drastic reduction of the Gruneisen parameter relates to the increased anharmonic contributions. Interestingly, as shown in Figure 3, the measured phonon's energies, and in particular those of the LO mode, are higher than what is expected according to the QHA predictions. Both the third and fourth terms of the interatomic potential contribute to the real part of the phonon self-energy, respectively, decreasing and increasing the phonon energies. There where QHA calculations well predict phonon energies, the two terms of higher order compensate each other. Our results suggest that for increasing temperature, cubic and quartic terms of the crystal Hamiltonian do not compensate anymore, with the progressive prevalence of the latter one. Further, more extensive perturbative calculations over and extended temperature range will be necessary to quantitatively confirm this hypothesis.

Mode linewidths

The evolution of phonons widths with volume [Figure 3(b)] shows two different trends for high pressure and high-temperature data. The discontinuity observed for both the optical modes' widths seems located near ambient conditions.

In the high-temperature regime, the widths of the phonons increase monotonically because thermal energy allows atoms to move away from their equilibrium positions, exploring the actual shape of the lattice potential beyond the quadratic well. In

other words, by increasing temperature, it is possible to check the degree of anharmonicity of the system and the weight of higher order energy terms. In general, it has been observed that the temperature dependence of the phonons' widths on the third and fourth order of the potential expansion has different trends. For the former the trend becomes linear over a few tens of Kelvin, while no linearity is observed for the latter as accurately show in a recent work were calculations are done up to temperatures around 1000 K at room pressure [39]. In our case, the high-volume experimental data, *i.e*, high temperature and room pressure phonon widths, reported in Figure 3(b), exhibit a linear behavior on temperature that is maintained up to 2000 K when adding literature data [17] (please see Supplemental Material Figure S2 for an extended view). This would suggest that four-phonons scattering has not a strong effect. However, the discrepancy between measured and computed data is not constant on temperature, differently from what observed on pressure. Moreover, the computed linewidths for the LO phonon show a clear deviation from linearity for temperatures higher than 1000 K. These finding support the hypothesis that the four-phonons scattering becomes not negligible with increasing temperature at room pressure non only for phonon energies, as discussed in the previous section, but also for phonon widths with a particular weight for the highest energy modes.

Compared with temperature, high pressure could be speculated to have an opposite effect, reducing interatomic distances, and enhancing the repulsive component in the interatomic potential, and hence, in some sort, increasing the harmonic character of the collective vibrations. This is qualitatively compatible with the almost constant or slight decrease of the width of the TO mode with decreasing volume caused by the increasing pressure. However, this is not the case for the LO mode, which shows an evident non-monotonic increase with decreasing volume, with a maximum width when LO energy matches that of ESW. This picture becomes clear once combining the theoretical and experimental results. The calculated MgO phonon density of states (DOS) reported in Figure 7 features two main energy pockets, one highly populated by phonon states belonging to TO and LA branches, the other by phonons belonging to TA branches, which all display a nearly flat dispersion (please refer to [31] for phonon dispersions and a more detailed description).

These two energy pockets, which evolve following the phonon band structure, *i. e.* blueshift decreasing the cell volume, host the final states of multiphonon decay processes (almost irrespective of the actual exchange momentum).

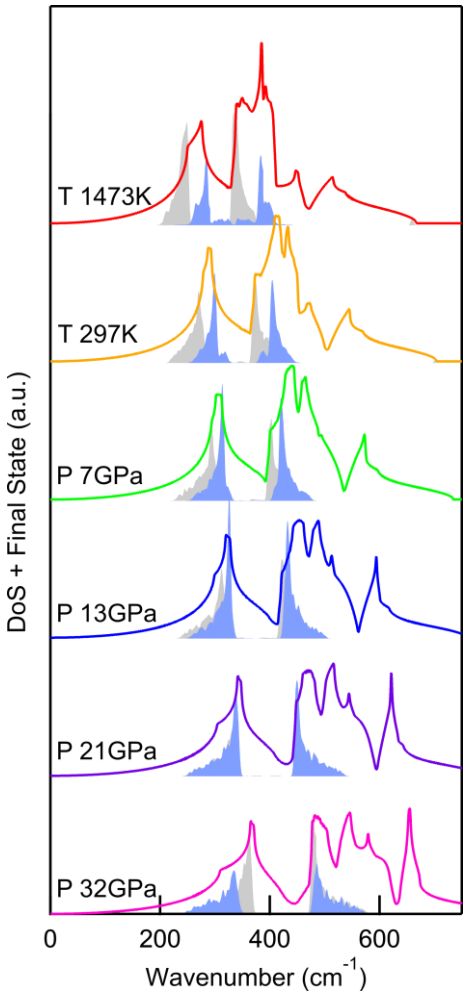

Figure 7. Evolution of the phonon DoS with the thermodynamic conditions. The color coding is consistent with marks in Figure 3. The blue (grey) shaded zone represents the final states of the LO (ESW) decay process.

If a particle, be this a photon or a phonon, possesses an energy equal to the sum of these two energies it can decay generating two phonons: this is what happens to the LO phonon or to photons having the ESW energy. At ambient conditions, the energies of the two pockets sum up to 650 cm^{-1}, and only photons satisfy the energy (and momentum) conservation. As the pressure increases, the band structure rearranges, the ESW approaches the LO energy that eventually matches the sum of the DOS energy pockets, thus providing an effective channel for the LO phonon to decay. The direct consequence is a progressive decrease in the LO lifetime that manifests with the observed increase in the linewidth. At the best energy matching, final states of ESW and LO decay processes superimpose (21 GPa, 790 cm^{-1}) and the LO width goes through a maximum. As the pressure further increases, the LO energy detunes, and

its width reduces. In conclusion, the presence of these pockets in the DOS, whose energy combination is tuned with one of the normal lattice modes, triggers multiphoton decay processes. The presence of such multiphoton processes increases the linewidth of normal modes and hence the anharmonicity of the lattice dynamics even at high pressure, where the stiffer and more packed environment should result in more harmonic lattice dynamics (*e.g.* [35]).

Conclusions

In this paper, we present a thorough experimental and numerical investigation of phonon optical modes of MgO as a function of temperature (from 300 to 1400 K) and pressure (from 0 to 21 GPa). The infrared reflectivity measurements complement previous datasets [17,38], allowing for a more detailed analysis, in particular at high pressure. Both phonon energies and phonon widths of three active phonon processes (LO, TO and ESW, an Excess of Spectral Weight caused by multiphonon processes) are probed over a variation of the unit cell volume exceeding 20%. The experimental results provide a critical testbench for the *ab-initio* simulations.

While the theoretical approach is overall validated in terms of optical phonon energy positions, calculations work better for TO than for LO. This can be ascribed to known limitations in the modeling of the effective charges and dielectric constant that lead to underestimation of the LO-TO splitting in MgO. Based on the comparison of our experimental and theoretical results we propose an empirical analytical expression for $Z^{*2}/\varepsilon_\infty$ as a function of the atomic unit cell volume V to rescale results from quasi-harmonic calculations.

Calculations within QHA account well for the volume dependence of the optical phonon energies observed in high-pressure experiments but fail both for TO and LO at larger volumes, corresponding to the highest investigated temperature. Higher-order, non-harmonic terms in the crystal Hamiltonian become necessary, with the quartic term expected to dominate over the cubic one.

Phonon widths were calculated beyond a quasi-harmonic approximation, including phonon-phonon scattering up to the third order of the lattice potential expansion. The results of these calculations reproduce remarkably well the non-trivial dependence on the lattice volume of both TO and LO phonon's linewidths highlighted by the experiments. Even if the absolute values do not closely match, the increase in the linewidths by almost a factor of 3 at large volumes is well captured. Furthermore, the almost constant mismatch suggests it might have an extrinsic origin. Interestingly, the calculations allow explaining the maximum in LO phonon widths versus pressure at around 21 GPa as the consequence of the progressive opening and closing of phonon decay channels, triggered by the energy of the ESW approaching and moving out that of LO phonon.

The highly non-linear evolution of phonon linewidth with volume could have important consequences for the lattice thermal conduction of MgO. More generally, predictions of lattice conduction of insulating crystals of geophysical interest based on a quasi-harmonic approach might fail at providing reliable estimates, as more complex models are required to properly describe lattice dynamics

Looking further in perspective, peculiar band structures such as those of MgO can be reverse engineered to tailor the desired set of final states and hence trigger decay processes of a given phonon branch, eventually at a given k-point of the reciprocal space. These customized materials will find applications based on fine control of the lattice transport properties in a given energy (temperature) range or along a given direction. Additionally, the temperature evolution of the band structure could be further exploited to set a temperature threshold for the activation/deactivation of the aforementioned decay processes.

All these fascinating applications call for an improved understanding of the anharmonic mechanisms controlling lattice vibrations.

Acknowledgment

The authors wish to thank Benoit Baptiste for single crystal alignment. This work was supported by the Investissements d'Avenir programme (reference No. ANR-11-IDEX-0004-02) and more specifically within the framework of the Cluster of Excellence MATeriaux Interfaces Surfaces Environnement (MATISSE) led by Sorbonne Université, by the China Scholarship Council – Sorbonne Université program for doctoral scholarships, and by the Conseil Régional d'Île-de-France through the DIM OxyMORE. HPC resources are granted under the GENCI Allocation No. A0030907320. Femtosecond laser micro-machining at the Institute de Minéralogie de Physique des Matériaux et de Cosmochimie (IMPMC), Paris has been developed and realized by the "Cellule Project" with the financial support of ANR 2010-JCJC-604-01. Infrared measurements were recorded during the accepted Proposals No. 20151247 and No. 20191644 on the Ailes beamline of synchrotron SOLEIL.

References:

[1] T. M. Tritt, *Thermal Conductivity* (Springer, Boston, 2004).
[2] R. A. Cowley, Adv. Phys. **12**, 421 (1963).
[3] A. M. Hofmeister, Science **283**, 1699 (1999).
[4] N. De Koker, Phys. Rev. Lett. **125902**, 1 (2009).
[5] N. de Koker, Earth Planet. Sci. Lett. **292**, 392 (2010).
[6] X. Tang and J. Dong, Proc. Natl. Acad. Sci. U. S. A. **107**, 4539 (2010).
[7] Y. Shen, C. N. Saunders, C. M. Bernal, D. L. Abernathy, M. E. Manley, and B. Fultz, Phys. Rev. Lett. 125, 085504 (2020).
[8] L. Lindsay, C. Hua, X. L. Ruan, and S. Lee, Mater. Today Phys. **7**, 106 (2018).
[9] F. Soubiran and B. Militzer, Phys. Rev. Lett. **125**, 175701 (2020).
[10] T. Feng, L. Lindsay, and X. Ruan, Phys. Rev. B **96**, 161201 (2017).
[11] W. Wan, Y. Ge, and Y. Liu, Appl. Phys. Lett. **114**, 031901 (2019).
[12] Y. Oba, T. Tadano, R. Akashi, and S. Tsuneyuki, Phys. Rev. Mater. **3**, 033601 (2019).
[13] D. Tristant, A. Cupo, X. Ling, and V. Meunier, ACS Nano **13**, 10456 (2019).
[14] F. Liu, P. Parajuli, R. Rao, P. C. Wei, A. Karunarathne, S. Bhattacharya, R. Podila, J. He, B. Maruyama, G. Priyadarshan, J. R. Gladden, Y. Y. Chen, and A. M. Rao, Phys. Rev. B **98**, 224309 (2018).
[15] Y. K. Peng, Z. Y. Cao, L. C. Chen, N. Dai, Y. Sun, and X. J. Chen, J. Phys. Chem. C **123**, 25509 (2019).
[16] R. Peierls, Ann. Phys. **395**, 1055 (1929).
[17] J. R. Jasperse, A. Kahan, J. N. Plendl, and S. S. Mitra, Phys. Rev. **146**, 526 (1966).
[18] J. Bouchet, F. Bottin, V. Recoules, F. Remus, G. Morard, R. M. Bolis, and A. Benuzzi-Mounaix, Phys. Rev. B **99**, 094113 (2019).
[19] Y. Zhao and D. L. Anderson, Phys. Earth Planet. Inter. **85**, 273 (1994).
[20] E. Mattern, J. Matas, Y. Ricard, and J. Bass, Geophys. J. Int. **160**, 973 (2005).
[21] B. Li and J. Zhang, Phys. Earth Planet. Inter. **151**, 143 (2005).
[22] D. Valencia, R. J. O'Connell, and D. Sasselov, Icarus **181**, 545 (2006).
[23] H. Marquardt, S. Speziale, H. J. Reichmann, D. J. Frost, F. R. Schilling, and E. J. Garnero, Science **324**, 224 (2009).
[24] F. Cammarano, H. Marquardt, S. Speziale, and P. J. Tackley, Geophys. Res. Lett. **37**, 03308 (2010).
[25] D. Antonangeli, J. Siebert, C. M. Aracne, D. L. Farber, A. Bosak, M. Hoesch, M. Krisch, F. J. Ryerson, G. Fiquet, and J. Badro, Science **331**, 64 (2011).
[26] G. M. Manthilake, N. De Koker, D. J. Frost, and C. A. Mccammon, Proc. Natl. Acad. Sci. U. S. A. **108**, 17901 (2011).
[27] X. Tang and J. Dong, Phys. Earth Planet. Inter. **174**, 33 (2009).
[28] H. Dekura and T. Tsuchiya, Phys. Rev. B **95**, 184303 (2017).
[29] H. C. Ryu, M. H. Kwak, S. B. Kang, S. Y. Jcong, M. C. Pack, K. Y. Kang, S. J. Lee, S. E. Moon, and S. O. Park, in *Integr. Ferroelectr.* **95**, 83, pp. 83–91.
[30] See Supplemental Material at [URL will be inserted by publisher] for detailed methods and analysis.
[31] P. Giura, L. Paulatto, F. He, R. P. S. M. Lobo, A. Bosak, E. Calandrini, L. Paolasini, and D. Antonangeli, Phys. Rev. B **99**, 220304(R) (2019).
[32] H. A. Kramers, Atti Cong. Intern. Fis. (Transactions Volta Centen. Congr. **2**, 545 (1927).
[33] R. de L. Kronig, J. Opt. Soc. Am. **12**, 547 (1926).
[34] A. R. Oganov, M. J. Gillan, and G. D. Price, J. Chem. Phys. **118**, 10174 (2003).
[35] D. Antonangeli, M. Krisch, D. L. Farber, D. G. Ruddle, and G. Fiquet, Phys. Rev. Lett. **100**, 085501 (2008).
[36] E. Grüneisen, Ann. Phys. **344**, 257 (1912).
[37] O. L. Anderson, Geophys. J. Int. **143**, 279 (2000).
[38] J. Pellicer-Porres, A. Segura, C. Ferrer-Roca, J. A. Sans, and P. Dumas, J. Phys. Condens. Matter **25**, 505902 (2013).
[39] Xiaolong Yang, Tianli Feng, Joon Sang Kang, Yongjie Hu, Ju Li, and Xiulin Ruan, Rev. B **101**, 161202(R) (2020)
[40] D. L. Farber, D. Antonangeli, C. M. Aracne, and J. Benterou, High Press. Res. **26**, 1 (2006).
[41] A. Celeste, F. Borondics, and F. Capitani, High Press. Res. **39**, 608 (2019).
[42] P. Roy, M. Rouzières, Z. Qi, and O. Chubar, Infrared Phys. Technol. **49**, 139 (2006).
[43] A. Voute, M. Deutsch, A. Kalinko, F. Alabarse, J.-B. Brubach, F. Capitani, M. Chapuis, V. Ta Phuoc, R. Sopracase, and P. Roy, Vib. Spectrosc. **86**, 17 (2016).
[44] J. P. Perdew, K. Burke, and M. Ernzerhof, Phys. Rev. Lett. **77**, 3865 (1996)

[45] M. Schlipf and F. Gygi, Comput. Phys. Commun. **196**, 36 (2015).
[46] T. J. B. Holland and R. Powell, J. Metamorph. Geol. **29**, 333 (2011).
[47] Y. Fei and Y. I. F. Ei, Am. Mineral. **84**, 272 (1999).
[48] S. Speziale, C.-S. Zha, T. S. Duffy, R. J. Hemley, and H. Mao, J. Geophys. Res. Solid Earth **106**, 515 (2001).
[49] M. Calandra, M. Lazzeri, and F. Mauri, Phys. C Supercond. Its Appl. **456**, 38 (2007).
[50] L. Paulatto, F. Mauri, and M. Lazzeri, **87**, 214303 (2013).
[51] L. Paulatto, I. Errea, M. Calandra, and F. Mauri, Phys. Rev. B - Condens. Matter Mater. Phys. **91**, 054304 (2015).

Supplemental Material to BY13452

Limits of quasiharmonic approximation in MgO: volume dependence of optical modes investigated by infrared reflectivity and *ab initio* calculations

Eugenio Calandrini[1], Lorenzo Paulatto[1], Daniele Antonangeli[1], Fei He[1], Ricardo P. S. M. Lobo[2,3], Francesco Capitani[4], Jean-Blaise Brubach[4], Pascale Roy[4], Laetitia Vincent[5], and Paola Giura[1,1*].

[1] *Sorbonne Université, Museum National d'Histoire Naturelle, UMR CNRS 7590, Institut de minéralogie, de physique des matériaux et de cosmochimie (IMPMC), 4 place Jussieu, F-75005 Paris, France*

[2] *LPEM, ESPCI Paris, PSL Univeristy, CNRS, F-75005 Paris, France*

[3] *Sorbonne Université, CNRS, LPEM, F-75005 Paris, France*

[4] *Synchrotron Soleil, L'Orme des Merisiers Saint Aubin, BP 48 91192, Gif-sur-Yvette , France*

[5] *Université Paris-Saclay, CNRS, Centre de Nanosciences et Nanotechnologie, C2N, Palaiseau 91120, France*

Materials and Methods

Materials:

Samples have been prepared starting from a crystallographic oriented single crystal of pure MgO with a size of 10x10x0.5 mm (Sigma-Aldrich) following a protocol similar to that described in [40]. After initial size reduction along easy cleavage directions, samples' thickness was reduced by mechanical polishing down to ~20 or ~60 μm depending on experiments, and subsequently, laser cut in a disk of the desired diameter to fit the experimental chamber of the Diamond Anvil Cell (DAC) (see later on).

Fourier Transform Infrared Spectroscopy:

Two different Fourier Transform Interferometers by Bruker were used to measure the MgO reflectivity: an IFS66v for measurements at high temperature and an IFS125 for measurements at high pressure. To cover the spectral window of interest, which extends from 300 to 900 cm^{-1}, interferometers were operated in two different configurations: one for the Far Infrared (FIR) region (100-600 cm^{-1}), and one for the Mid Infrared (MIR) region (500-6000 cm^{-1}).

FIR measurements vs. T (P) exploited a coated multilayer beam-splitter, a Si bolometer detector cooled to liquid helium temperature, and a mercury (synchrotron) source for the IFs 66v/S (IFS 125) interferometer. MIR measurements exploited a KBr beam-splitter, an MCT (HgCdTe) detector cooled to liquid nitrogen temperature, and a globar (synchrotron) source for the IFs 66v/S (IFS 125) interferometer. Due to the high absorption of MgO, spectra were recorded in reflection configuration. For each temperature (pressure), the reflectance spectrum was obtained through the ratio between the light intensity reflected by the pristine surface of the sample and the one reflected by a reference. For

* 1 Corresponding author : paola.giura@sorbonne-universite.fr

the high-temperature measurements, the reference was acquired on a subsequent run on the gold-evaporated sample surface. High-pressure data were collected in two distinct experimental runs: a first for the pressure range 5-21 GPa (here-after "HP-run") and a second for the pressure range 1-5 GPa (here-after "LP-run"). For the "HP-run" the recovered sample was gold-coated and measured again at high pressures to provide the reference. In the "LP-run" a gold foil with a size comparable to that of the sample was placed on the side of the gasket and measured just after the sample at each pressure point.

Sample Environment:

High temperatures were generated by a Linkam TS1500 temperature-controlled stage placed at the focus of the infrared Bruker Hyperion 1000 microscope, equipped with the IFS 66v/S interferometer, at the LPEM laboratory of the ESPCI.

High pressure was generated by membrane-driven DACs. Depending on the target frequency range, the resulting spot size, and the pressure range, different DAC setups and pressure transmitting medium (PTM) [41] were used. In the "HP-run" for the FIR, the DAC was equipped with 500 μm culets diamonds and rhenium gasket, pre-indented to a thickness of 55 μm, and with a hole of 250 μm in diameter acting as the sample chamber. A 20 μm thick MgO disk of 220 μm diameter was loaded together with a ruby chip, using pure polyethylene (PE) as a PTM. For the MIR, the DAC was equipped with 300 μm culets diamonds, and a 120 μm diameter MgO disk was loaded together with a ruby chip in a 150 μm diameter chamber, using Ar as PTM. For the "LP-Run" the same cell was employed for both FIR and MIR measurements, equipped with 600 μm culets diamond pressing on a 300 μm diameter chamber containing a MgO disk, 200 μm wide and 60 μm thick, a ruby chip, and CsI as PTM. In all runs, the pressure was monitored in-situ through ruby fluorescence. Measurements were performed at the IR beamline AILES [42, 43] of SOLEIL synchrotron, using a homemade microscope compartment equipped with two Schwarzschild objectives connected to the IFS125 interferometer.

Dielectric function and reflectivity: Lorentz model and Kramers-Kronig relations:

Within the framework of the Lorentz model, the complex dielectric function $\tilde{\varepsilon} = \varepsilon_1 + i\varepsilon_2$ is described by a set of Lorentzian oscillators and assumes the following form:

$$\varepsilon_1 = n^2 - k^2 = \varepsilon_\infty + \sum_i \frac{S_i \omega_i^2 (\omega_i^2 - \omega^2)}{(\omega_i^2 - \omega^2)^2 + \Gamma_i^2 \omega^2} \; ;$$
$$\varepsilon_2 = 2nk = \sum_i \frac{S_i \omega_i^2 \Gamma_i \omega}{(\omega_i^2 - \omega^2)^2 + \Gamma_i^2 \omega^2} \quad (1)$$

where ε_∞ is the high-frequency dielectric constant, S_i the strength, Γ_i the damping constant or the inverse of the lifetime ($\Gamma_i = 1/\tau_i$) and ω_i the frequency of the *i-th* resonance. In the case of MgO, 2 resonances are defined: one related to the TO phonons, to which IR spectroscopy has direct access, and one assigned *ad hoc* to account for the ESW. ε_∞ is kept constant as reported in reference [17] of main text. The complex refractive index $\tilde{n} = n + ik$ is connected to the reflectivity R of unpolarized radiation at normal angle of incidence through:

$$R = \frac{(n - n_{host})^2 + k^2}{(n + n_{host})^2 + k^2} \qquad (2)$$

where n_{host} is the refractive index of the host environment, in our case 1 (air) for the high-temperature measurements and 2.41 (diamond) for the high-pressure measurements. Representative curves of this

fitting procedure are superimposed to the corresponding measured spectra as red dashed lines in Figure 1. Known the dielectric constant, the imaginary part of the energy loss function $\varepsilon_2/(\varepsilon_1^2+\varepsilon_2^2)$ provides the frequency and linewidth of LO phonons.

A model-independent analysis relying on the causality principle can be done on the basis of the Kramers-Kronig transformations (KK) [32,33]. KK transformations provide the full complex dielectric constant once the normal-incidence reflectance is known at all frequencies. From the obtained reflectance, $R(\omega)$, it is then possible to obtain the phase and, subsequently, the real and imaginary parts of the refractive index as:

$$\theta(\omega) = -\frac{1}{\pi} P \int_{-\infty}^{+\infty} \frac{\ln\sqrt{R(\omega')}}{\omega'-\omega} d\omega'$$

$$n = \frac{1-R(\omega)}{1+R(\omega)+2\sqrt{R(\omega)}\cos\theta(\omega)}$$

$$k = \frac{2\sqrt{R(\omega)}\sin\theta(\omega)}{1+R(\omega)+2\sqrt{R(\omega)}\cos\theta(\omega)}$$

Once obtained the real and imaginary part of the refractive index n, it is possible to derive the dielectric function as described in (1). Red curves in panels a and e of Figure 2 of the main text report the imaginary part (to highlight the position of TO phonon) and the energy loss function (to highlight the position of LO phonon) resulting from the KK. Due to the integral nature of the KK transformations, the uncertainty of the spectral shape of the dielectric constant at a given frequency is almost entirely related to the experimental uncertainty on R(ω) at that frequency. The uncertainty of the absolute value of the dielectric constant is due to the value of the R(ω) integrated over all frequencies.

Density Functional Perturbation Theory:

Mg and O are described using optimized norm-conserving Vanderbilt pseudopotentials [44,45]. Electronic exchange and correlation are approximated with the Perdew–Burke-Ernzerhof functional [44]. Lattice parameters of the cubic rock salt crystal structure were determined according to a third-order Birch-Murnaghan equation of state, with the thermal pressure modeled following reference [46] and given as input to the calculations. The volume at ambient condition V_0 and the thermal expansion coefficient α were experimentally determined during the measurements presented in reference [31]; for the bulk modulus and its derivative, K and K', we used the values reported in reference [47] and for the Einstein temperature Θ_0, the Gruneisen parameter γ_0 and Gruneisen power law β, the ones in reference [48].

Phonons energy dispersions were calculated in quasi-harmonic (QHA) approximation using the experimental lattice parameters. Phonon widths due to intrinsic phonon-phonon scattering were calculated treating the 3rd order of the lattice potential expansion [49-51].

Supplementary Figures

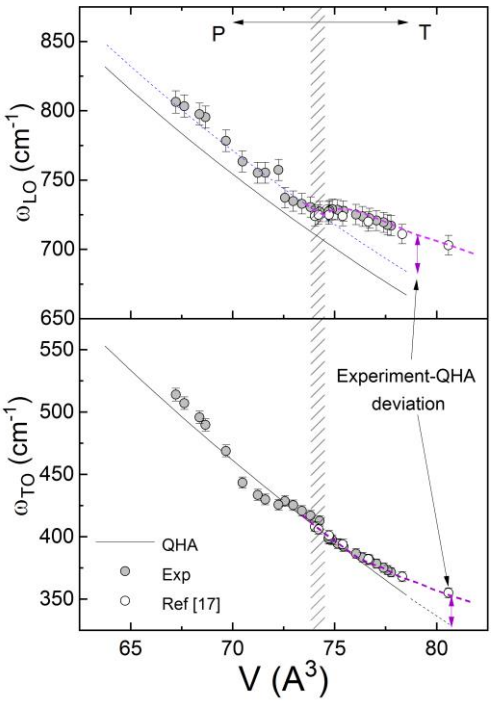

Figure S1. Phonon energies as a function of the unit cell volumes. Shaded gray area highlights volumes covered by both high-pressure, ambient-temperature measurements (otherwise on the left) and low-temperature, ambient-pressure measurements (ref [17] of main text). High-temperature ambient-pressure measurements are on the right. Full circles are present experiments, open circles are experimental values from the literature (ref [17] of main text). Solid lines are results from QHA calculations. The dashed line corresponds to QHA values for the LO phonon rigidly translated to match the experiments. Bold dashed violet lines are guides for the eyes highlighting the experimental deviation at large volumes (high temperatures) from QHA predictions.

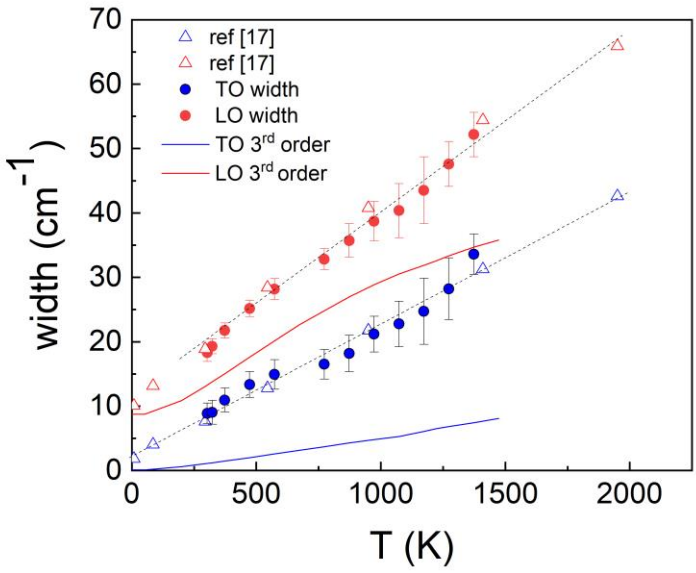

Figure S2. Longitudinal (red) and transverse (blue) phonon widths as a function of temperature. Solid circles are our IR data; open triangles are IR data from literature (ref [17] of main text); solid lines are DFPT calculation including 3-phonons scattering. Black dashed linear lines are guides for the eyes.

References

[40] D. L. Farber, D. Antonangeli, C. M. Aracne, and J. Benterou, High Press. Res. **26**, 1 (2006).

[41] A. Celeste, F. Borondics, and F. Capitani, High Press. Res. **39**, 608 (2019).

[42] P. Roy, M. Rouzières, Z. Qi, and O. Chubar, Infrared Phys. Technol. **49**, 139 (2006).

[43] A. Voute, M. Deutsch, A. Kalinko, F. Alabarse, J.-B. Brubach, F. Capitani, M. Chapuis, V. Ta Phuoc, R. Sopracase, and P. Roy, Vib. Spectrosc. **86**, 17 (2016).

[32] H. A. Kramers, Atti Cong. Intern. Fis. (Transactions Volta Centen. Congr.) **2**, 545 (1927).

[33] R. de L. Kronig, J. Opt. Soc. Am. **12**, 547 (1926).

[44] J. P. Perdew, K. Burke, and M. Ernzerhof, Phys. Rev. Lett. **77**, 3865 (1996).

[45] M. Schlipf and F. Gygi, Comput. Phys. Commun. **196**, 36 (2015).

[46] T. J. B. Holland and R. Powell, J. Metamorph. Geol. **29**, 333 (2011).

[31] P. Giura, L. Paulatto, F. He, R. P. S. M. Lobo, A. Bosak, E. Calandrini, L. Paolasini, and D. Antonangeli, Phys. Rev. B **99**, 220304(R) (2019).

[47] Y. Fei and Y. I. F. Ei, Am. Mineral. **84**, 272 (1999).

[48] S. Speziale, C.-S. Zha, T. S. Duffy, R. J. Hemley, and H. Mao, J. Geophys. Res. Solid Earth **106**, 515 (2001).

[49] M. Calandra, M. Lazzeri, and F. Mauri, Phys. C Supercond. Its Appl. **456**, 38 (2007).

[50] L. Paulatto, F. Mauri, and M. Lazzeri, Phys. Rev. B **87,** 214303 (2013).

[51] L. Paulatto, I. Errea, M. Calandra, and F. Mauri, Phys. Rev. B - Condens. Matter Mater. Phys. **91**, 054304 (2015).